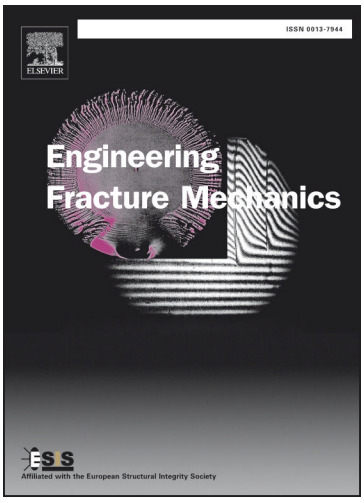


# Modelling fracture on polyolefin fibre reinforced concrete specimens subjected to mixed-mode loading

F. Suárez, J.C. Gálvez, A. Enfedaque, M.G. Alberti

PII: S0013-7944(18)31331-6
DOI: https://doi.org/10.1016/j.engfracmech.2019.02.018
Reference: EFM 6359

To appear in: *Engineering Fracture Mechanics*

Received Date: 28 November 2018
Accepted Date: 11 February 2019

Please cite this article as: Suárez, F., Gálvez, J.C., Enfedaque, A., Alberti, M.G., Modelling fracture on polyolefin fibre reinforced concrete specimens subjected to mixed-mode loading, *Engineering Fracture Mechanics* (2019), doi: https://doi.org/10.1016/j.engfracmech.2019.02.018

# Modelling fracture on polyolefin fibre reinforced concrete specimens subjected to mixed-mode loading

F. Suárez[a], J.C. Gálvez[b], A. Enfedaque[b], M.G. Alberti[b]

[a]*Departamento de Ingeniería Mecánica y Minera. Universidad de Jaén. Campus Científico-Tecnológico de Linares. Cinturón Sur 23700-Linares (Jaén)*

[b]*Departamento de Ingeniería Civil- Construcción. Universidad Politécnica de Madrid . E.T.S.I. Caminos, Canales y Puertos, C/ Profesor Aranguren s/n 28040 – Madrid, Spain*

**Abstract**

In recent years, polyolefin fibres have proved a remarkable performance as reinforcement of concrete, which has inspired a number of studies involving, among others, the simulation of fracture on polyolefin fibre reinforced concrete (PFRC) specimens. Fracture has been successfully reproduced on PFRC specimens in the past by means of an embedded crack model with a trilinear softening fucntion, but always using for comparison the classical three-point bending test, which employs a symmetrical setup and induces fracture under pure mode I conditions. In the present study, six sets of specimens tested under an alternative setup of the three-point bending test, which induces fracture under mixed-mode conditions (I and II) are simulated using the same numerical approach. The results not only prove that the use of a trilinear softening function together with an embeded cohesive crack approach can reproduce fracture under mixed-mode conditions, but also provide interesting insights on how the trilinear softening function may be designed for suiting the usage of different fibre lengths or varying the proportions of polyolefin fibres.

*Keywords:* Mixed-mode fracture, Fibre-reinforced concrete, Polyolefin fibres, Embedded cohesive crack model

## 1. Introduction

In the last years, there has been an increasing interest in studying how the addition of different types of fibres modifies the behaviour of concrete [1, 2, 3, 4, 5, 6]. Apart from steel fibres, that have been used as fibre reinforcement for decades [7], in the last years new materials have been analysed as possible fibre reinforcement for structural concrete elements. The use of these materials tries to overcome the main drawbacks that appear with the use of steel fibres, especially regarding corrosion, which can not only affect the durability but also affects their aesthetical aspect. The appearance of new recommendations in several Standards [8, 9] regarding fibre-reinforced concrete has boosted the interest in this technology.

One of the materials that has proved to be a good choice as fibre-reinforcement of concrete is polyolefin, a polymer that, when used in the form of macro-fibres and in a proper proportion, greatly increases the performance of concrete under tensile stresses [10, 11, 12, 13]. Regarding this type of fibres, their use with conventional vibrated concrete and self-compating concrete, as well as the influence of the fibre proportion on the mechanical properties of the mix in fresh and in hardened states have been studied in the past. Other aspects, including the combination of these fibres with steel fibres [14] or the influence of the orientation of fibres in the mix on the effectiveness of them [15] have also been covered.

In order to study the fracture behaviour of different concrete mixes, the specimens have been usually analysed by means of a classical three-point bending test [16], where the supports and the actuator that loads the specimen are disposed symmetricaly (see Figure 1), leading to the initiation and development of cracking under pure mode I conditions. In these cases, the numerical simulation of fracture has been

*J.C. Gálvez
*Email address:* jaime.galvez@upm.es (J.C. Gálvez)

successfully carried out by means of cohesive crack zone modelling and using a trilinear softening function that is able to reproduce the load recovery after the cracking of the concrete matrix and later decrease of the load bearing capacity, typical of these mixes [17, 18].

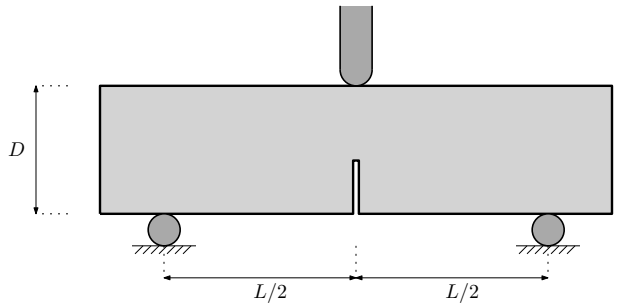


Figure 1: Experimental setup of a classical three-point bending test.

Fracture mechanics to characterise the behaviour of quasi-brittle materials such as concrete are widely required in order to avoid brittle failure in construction structures. In such a sense, not only pure Mode I and Mode II must be studied for a complete characterization. In such a sense, deeper knowledge of the behaviour under mixed-mode I/II of fracture is of significant interest given that most of the structures are subjected to a combination of stresses as has been studied for fibre reinforced concrete in recent research [19, 20].

In the present work the same model is adopted to reproduce fracture in specimens subjected to three-point bending tests where the loading actuator and the supports are placed unsymmetrically in order to induce fracture under a combination of modes I and II. These tests were used in the past with unreinforced concrete [21] and are here applied to polyolefin fibre reinforced concrete specimens. The model is used to numerically reproduce fracture with two sets of specimens: in the first set, all the specimens are of the same size and three polyolefin fibre dosages are studied: 3, 6 and 10 kg/m$^3$, while in the second set three specimen sizes are tested, all of them with a fixed fibre proportion of 10 kg/m$^3$. Cohesive materials, such as concrete and mortar, show a size effect under fracture conditions; the cohesive crack model has been successful in simulating this behaviour [22].

The use of trilinear softening functions has proven to be effective in both sets of tests. In the case of specimens with an increasing proportion of fibres, the softening functions are similar in the beginning and differ in the last part, where the increase of fibres help to reach higher post-peak strengths. As for the set of specimens of different sizes, fracture can be reproduced in all of them using a single softening function. This is a key point, since softening functions obtained with standardised tests allow to predict the fracture behaviour of specimens with distinct sizes; in this sense, it might be said that the cohesive crack approach adopted in this work is a predictive tool that reproduces the fracture size effect.

## 2. Design of the study

One of the main issues to be studied regarding polyolefin-fibre reinforced concrete (PFRC) is the distribution of fibres inside the mix. In previous works the influence of borders has been identified in what has been referred to as *wall effect* [23, 15]. Due to evident geommetrical issues, the macroscopic nature of the fibres suggests that the specimen size may be important regarding the scalability of the experimental results, since a size effect may be expected on the mechanical properties of the mix. The influence of the fibre length has also been studied in the past [24], proving that the fibre effectiveness greatly depends on the embedded length of the fibres crossing a crack, similarly to the anchorage length of steel rebars in conventional reinforced concrete. A deeper review on this topic can be found in [25].

In this work, two sets of specimens were tested under mixed-mode fracture conditions. The first set of specimens were manufactured with the same concrete dosage and different fibre proportions, with all specimens being of the same dimensions (600 mm×150 mm×150 mm); this set of specimens was designed to check the validity of the cohesive crack approach for mixed-mode fracture with increasing fibre proportions. The second set of specimens had the same fibre dosage and are of different sizes, keeping the aspect ratio

in the specimen plane; this set was designed to observe possible size effects that should be considered when modelling fracture.

It should be noted that, although fracture has been successfully reproduced in PFRC specimens in the past, all previous models have dealt with pure mode I fracture, which was induced by the classical symmetric three-point bending test [16]. Here, a modified version of the test was used to induce fracture under a combination of mode I and mode II conditions, so that the validity of trilinear softening functions used with the cohesive crack approach could be verified.

## 3. Experimental results

### *3.1. Materials and concrete mixes*

As mentioned before, two sets of specimens have been tested; Table 1 shows the mix proportioning and fibre dosage of each concrete. In the case of the first set, three mixes are referred (FC-3, FC-6 and FC-10), all of them with the same proportions of concrete components and only differing in the polyolefin fibre dosage. Regarding the second set of specimens, all of them were manufactured with the same concrete formulation and fibre proportion (10 kg/m$^3$) and only differed in the specimen dimensions, as will later be detailed. It should be noted that in all cases the water/cement ratio is constant.

Table 1: Proportioning of each mix analysed in this study.

| | Cement (kg/m$^3$) | Limestone powder (kg/m$^3$) | Water (kg/m$^3$) | Sand (kg/m$^3$) | Gravel (kg/m$^3$) | Grit (kg/m$^3$) | Superplasticizer (% cem. weight) | Polyolefin fibres (kg/m$^3$) |
|---|---|---|---|---|---|---|---|---|
| FC-3 | 375 | 100 | 187.5 | 916 | 300 | 450 | 2.8 | 3 |
| FC-6 | 375 | 100 | 187.5 | 916 | 300 | 450 | 2.8 | 6 |
| FC-10 | 375 | 100 | 187.5 | 916 | 300 | 450 | 2.8 | 10 |
| SCC | 375 | 200 | 187.5 | 918 | 367 | 245 | 4.7 | 10 |

### *3.2. Specimens*

Table 2 shows the dimensions of each group of specimens, as well as the nomenclature used in each case. Please, note that the nomenclature of the specimens of the first set, FC, refers to the clasification of the consistency of the mix: *fluid concrete*. In the case of the specimens of the second set, SCC refers to *self-compacting concrete* and letters L, M and S refer to the specimen sizes (large, medium and small, respectively). In these specimens, the width was reduced in order to ease the specimens handling.

Table 2: Nomenclature, dimensions, concrete type and fibre lengths used for each set of specimens.

| Nomenclature | Dimensions (mm) | | | Concrete type | Fibre |
|---|---|---|---|---|---|
| | Length | Width | Height | type | length (mm) |
| FC-3 | 600 | 150 | 150 | Fluid | 60 |
| FC-6 | 600 | 150 | 150 | Fluid | 60 |
| FC-10 | 600 | 150 | 150 | Fluid | 60 |
| SCC-S | 340 | 50 | 75 | Self-compacting | 48 |
| SCC-M | 675 | 50 | 150 | Self-compacting | 48 |
| SCC-L | 1350 | 50 | 300 | Self-compacting | 48 |

### *3.3. Experimental setup*

The experimental setup corresponded to type 1 disposition described by Gálvez et al. in [21], where the classical three-point bending test was modified changing the disposition of supports and load in order to induce a crack initiation and development under a combination of modes I and II. Figure 2 shows the geommetry of the experimental setup. Note that although there were slight differences in specimen proportioning, the experimental setup was exactly the same between the supports, where all the cracking process takes place; such changes in the specimens dimensions might not be considered relevant for the type of analysis performed.

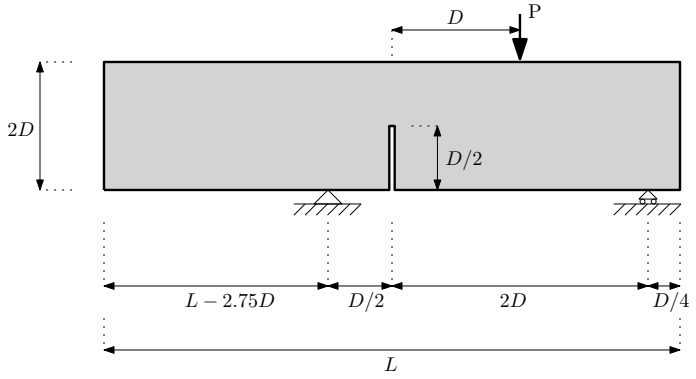


Figure 2: Dimensions of the nonsymmetric three-point bending test in terms of height $D$.

## 4. Numerical work

In this section the numerical work is presented. In the first place, the embedded crack formulation is briefly introduced and later the especific models prepared for this study are presented, providing a brief description of the meshes used and the material parameters considered.

### *4.1. Embedded cohesive crack model*

The crack initiation and development is modelled by means of a formulation that, although initially designed for concrete [26, 22], has also been adapted with success to non isotropic materials, such as brickwork masonry elements [27] and fibre-reinforced cementitious materials under pure mode I fracture conditions [17, 18].

Such formulation is based on the cohesive zone approach proposed by Dugdale [28] and Barenblatt [29] and later developed by Hillerborg [30] for a finite element formulation (for more information on this topic the reader is referred to [31]). It also relies on the fact that for most experiments found in the literature fracture develops under a predominant local mode I, therefore, assuming that the cohesive stress vector $\boldsymbol{t}$ is always perpendicular to the crack opening and paralell to the crack displacement vector $\boldsymbol{w}$, which is why it is usually referred to as a central forces model. This relationship can be expressed by (1).

$$\boldsymbol{t} = \frac{f(\tilde{w})}{\tilde{w}}\boldsymbol{w} \qquad \text{with } \tilde{w} = \max(|\boldsymbol{w}|) \tag{1}$$

where $f(|\tilde{w}|)$ stands for the material softening function, defined in terms of an equivalent crack opening $\tilde{w}$, which stores the maximum historical crack opening in order to account for possible unloading scenarios. In this case (PFRC specimens), this function presents three linear regions as depicted in Figure 3, and is defined by the following expression:

$$\sigma = \begin{cases} f_{ct} + \left(\dfrac{\sigma_k - f_{ct}}{w_k}\right) \cdot w & \text{if } 0 < w \leq w_k \\ \sigma_k + \left(\dfrac{\sigma_r - \sigma_k}{w_r - w_k}\right) \cdot (w - w_k) & \text{if } w_k < w \leq w_r \\ \sigma_r + \left(\dfrac{-\sigma_r}{w_f - w_r}\right) \cdot (w - w_r) & \text{if } w_r < w \leq w_f \\ 0 & \text{if } w > w_f \end{cases} \tag{2}$$

Although the formulation of the embedded crack element used in this study can be presented in a more general form (for more information on the numerical model the reader is referred to [22] and [26]), when constant strain triangular elements are employed, which is the case of the models shown later, cracking can only take place parallel to one of the triangle sides and at mid height. These conditions must be imposed in order to guarantee that both local and global equilibria are met. This leaves only three possible crack paths, as shown in Figure 4.

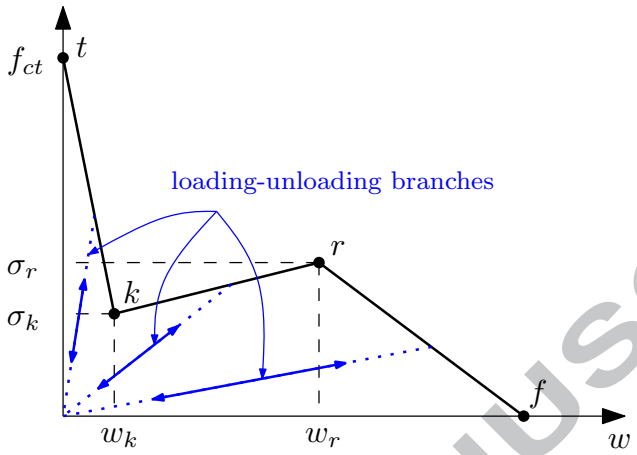


Figure 3: Scheme of a trilinear softening function.

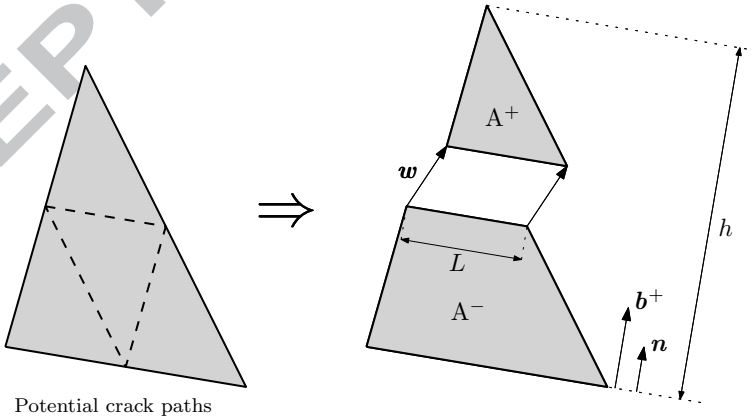


Figure 4: Potential crack paths (left) and geometrical definitions of $\boldsymbol{w}$, $\boldsymbol{n}$ and $\boldsymbol{b}^+$ (right).

Following the strong discontinuity approach, the element is divided into two parts, $A^+$ and $A^-$ and the stress vector $\boldsymbol{t}$ is constant along the crack and expressed by (3).

$$\boldsymbol{t} = \frac{A}{hL}\boldsymbol{\sigma}\cdot\boldsymbol{n} \tag{3}$$

where $A$ stands for the area of the element, $h$ for the height of the triangle over the side opposite to the solitary node, $L$ for the crack length in the element and $\boldsymbol{n}$ for the unit vector normal to that side and to the crack.

The material outside the crack is assumed to behave elastically and the crack displacement vector $\boldsymbol{w}$ is solved following an algorithm that is similar to that used in plasticity, since the stress tensor is obtained using a strain vector that results from substracting the contribution of the crack displacement to the apparent strain by means of (4)

$$\boldsymbol{\sigma} = \boldsymbol{E} : \left[\epsilon^a - \left(\boldsymbol{b}^+ \otimes \boldsymbol{w}\right)^S\right]\cdot\boldsymbol{n} \tag{4}$$

where $\boldsymbol{E}$ is the elastic tangent tensor, $\epsilon^a$ the apparent strain vector obtained with the nodal displacements, $\boldsymbol{b}^+$ the gradient vector of the shape function that corresponds to the solitary node, which can be easily obtained in this case by (5), superscript $S$ indicates the symmetric part of the resulting tensor, : the usual double-dot product ($(\boldsymbol{A}:\boldsymbol{b})_{ij} = A_{ijkl}b_{kl}$) and $\otimes$ the usual direct product ($(\boldsymbol{a}\otimes\boldsymbol{b})_{ij} = a_i b_j$).

$$\boldsymbol{b}^+ = \frac{1}{h}\boldsymbol{n} \tag{5}$$

Given that the stress vector $\boldsymbol{t}$ can be obtained by Cauchy's lemma through $\boldsymbol{t} = \boldsymbol{\sigma}\cdot\boldsymbol{n}$, substituting the stress tensor given by (4), this expression results into:

$$\frac{f(\tilde{w})}{\tilde{w}}\boldsymbol{w} = [\boldsymbol{E}:\boldsymbol{\epsilon}^a]\cdot\boldsymbol{n} - \left[\boldsymbol{E} : \left(\boldsymbol{b}^+\otimes\boldsymbol{w}\right)^S\right]\cdot\boldsymbol{n}$$

that can be rewritten in the form:

$$\left[\frac{f(\tilde{w})}{\tilde{w}}\boldsymbol{1} + \boldsymbol{n}\cdot\boldsymbol{E}\cdot\boldsymbol{b}^+\right]\cdot\boldsymbol{w} = [\boldsymbol{E}:\boldsymbol{\epsilon}^a]\cdot\boldsymbol{n} \tag{6}$$

where $\boldsymbol{1}$ stands for the second-order identity tensor.

The crack displacement is solved by means of the Newton-Raphson's method; for a certain set of nodal displacements, once the crack is formed, $\boldsymbol{b}^+$ and $\boldsymbol{n}$ are known, therefore, the iterative process can find the value of the crack opening $w$ that satisfies (6).

This model is numerically implemented by a user subroutine that runs using the commercial code ABAQUS and defines a material behaviour that follows the formulation presented above (UMAT subroutine). Since the formulation needs information of the geommetry of the elements to compute vectors $\boldsymbol{n}$, $\boldsymbol{b}^+$, crack length $L$ and the element area $A$, it reads this data from an external file that stores the geommetry of the model, nodes and elements.

### *4.2. Meshes and material parameters*

The experimental results have been numerically reproduced by means of the finite element method with bidimensional models using reduced integration triangular models, since this is a requisite of the formulation described before. The mesh is refined in the region where crack develops and remains coarse out of it in order to reduce the computational cost. All elements are assigned a material that follows the numerical behaviour described above, so if the principal stress in an element does not reach the critical value $f_{ct}$ it behaves elastically and if it reaches that critical value experiments softening according to a trilinear softening function. For the sake of illustration, Figure 5 shows one of the meshes used in this study where the cracking process has started.

The aim of the numerical models is to reproduce the experimental behaviour observed in each of the mixes, to do this, two diagrams have been used for comparison, the Load-CMOD and de Load-LVDT diagrams. The first of them represents the evolution of loading against the crack opening while the second represents loading against the vertical displacement of the loading point. The CMOD measurement (crack mouth

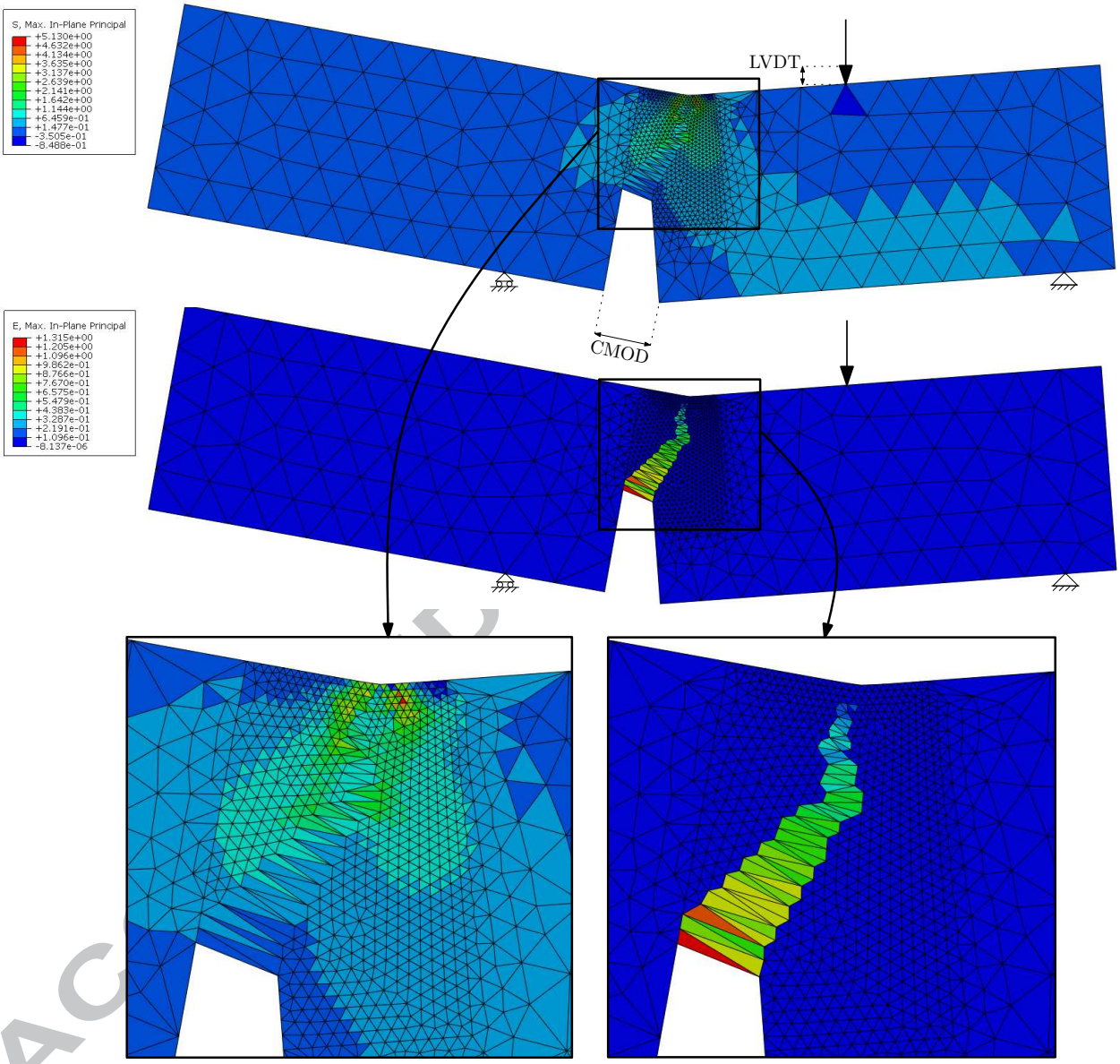


Figure 5: Deformed mesh of the SCC-L simulation showing the colour map of the main stresses in MPa (upper general figure), the colour map of the main strains (lower general figure) and details of the crack path for both maps.

Table 3: Characteristic points of the trilinear softening functions used with the fluid concrete mixes.

| | FC-3 | | | | FC-6 | | | | FC-10 | | | |
|---|---|---|---|---|---|---|---|---|---|---|---|---|
| | $t$ | $k$ | $r$ | $f$ | $t$ | $k$ | $r$ | $f$ | $t$ | $k$ | $r$ | $f$ |
| $w$ (mm) | 0.00 | 0.15 | 2.250 | 7.50 | 0.00 | 0.14 | 2.250 | 7.50 | 0.00 | 0.13 | 2.250 | 7.50 |
| $\sigma$ (MPa) | 2.30 | 0.12 | 0.245 | 0.00 | 2.30 | 0.33 | 0.700 | 0.00 | 2.30 | 0.75 | 1.700 | 0.00 |

Table 4: Characteristic points of the trilinear softening functions used with the sef-compacting concrete mixes.

| | SCC | | | |
|---|---|---|---|---|
| | $t$ | $k$ | $r$ | $f$ |
| $w$ (mm) | 0.000 | 0.070 | 1.650 | 7.500 |
| $\sigma$ (MPa) | 3.000 | 0.570 | 1.050 | 0.000 |

opening displacement) is experimentally measured by means of a strain gauge that provides the displacement between the points at the end of the notch (see Figure 5). It is worth noting that since the mixed-mode loading induces a non-symmetrical deformed shape of the specimen, the measured value combines the horizontal and vertical relative displacements of both points, which must be taken into account to extract the results from the numerical simulation. The value corresponding to the actuator vertical displacement is obtained by means of a linear variable differential transducer (LVDT) and provides the vertical displacement of the point where loading is applied (see Figure 5).

Regarding the trilinear softening functions, Tables 3 and 4 show the coordinates of the characteristic points used for each of the FC and SCC mixes; the shape of these functions can be observed in Figure 6. The following criteria has been followed for each group of specimens: to reproduce the results of the fluid concrete specimens (FC-3, FC-6 and FC-10), the initial and final points $t$ and $f$ (see Figure 3) are coincident in all cases, only varying the intermediate points $k$ and $r$ so that the curves can reproduce an increasing proportion of polyolefin fibres. In the case of SCC specimens, the same softening curve has been used for all specimen sizes, since all of them have the same proportion of fibres.

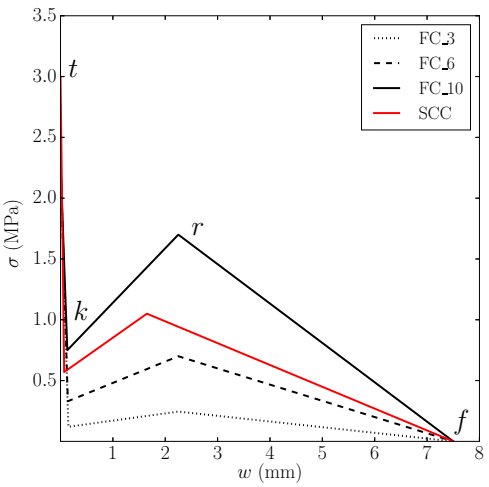


Figure 6: Trilinear softening diagrams used to simulate each mix.

It is worth mentioning that previous research [17] found that the position of the turning points of the softening curves might be computed predictively given that they are related with certain material properties. That is to say, $t$ is a value that can be assumed as the value of $f_{ct}$. The values of $k$, can be fitted by means of the evolution of the angle following an exponential function with the only influence of the volume fraction of fibres. With this angle, it is possible to compute the intersection on the straight line with such slope and the softening curve of plain concrete that corresponds with the point $k$. Concerning the coordinates of point $r$, some additional parameters seemed to influence in its value. Therefore, the number of pulled out fibres, the

orientation factor ($\theta$), the ultimate tensile strength ($\sigma_u$) of the fibres as well as the fibre dosage ($V_f$) could be used to simulate the stress value by following the expression (7).

$$\sigma_r = (1 - \%\text{Pulled-out}) \cdot V_f \cdot \theta \cdot \sigma_u \tag{7}$$

## 5. Results

Figure 7 shows the load-CMOD and load-LVDT curves for the FC specimens. Observing the load-CMOD curves it can be concluded that the softening functions shown in Figure 6 can reproduce with high degree of accuracy the peak load in all cases and also the load decrease after concrete matrix reaches its tensile capacity. As for the later behaviour, in all cases the numerical simulations remain inside the experimental envelope, reproducing the whole process of load recovery due to the work of the fibres once concrete capacity is exceeded and the load decrease once the action of the fibres reduces its effectiveness. Similar comments can be made for the Load-LVDT curves, which also show accuracy in the final unloading slopes.

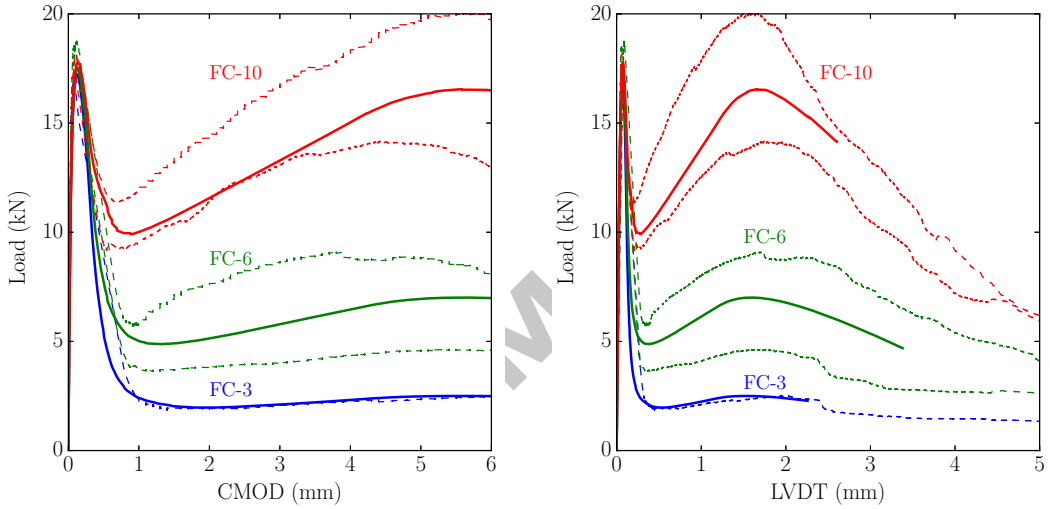


Figure 7: Load-CMOD and Load-LVDT diagrams for the fluid concrete specimens and simulations. Continuous lines represent the numerical results and dashed lines the experimental results.

Figure 8 presents the same diagrams for the SCC specimens. If the load-CMOD diagram is observed, the model reproduces well the overall behaviour of the mixes in all specimen sizes using the same softening function in all cases. Nevertheless, it is true that the peak load seems to be slightly overestimated for small specimens and underestimated for large specimens; although this could be corrected by modifying the $t$ and $k$ points in the trilinear function, in this case the softening function has been intentionally remained fixed for all sizes in order to see if the same material parameters could reproduce the experimental results with different specimen sizes. In the case of the load-LVDT curves, the same behaviour is observed. According to these results, it seems that the same trilinear softening function can reproduce well the fracture behaviour at different scales of the problem.

Regarding the trajectories of the cracks during the fracture process, it should be mentioned that it is remarkably influenced by the presence of fibres, not being regular or even parallel between the two faces of the specimen. Having said that, in average values – and assuming the direction of the crack as a line that compensated areas below and above – the inclining angle of FC-3, FC-6 and FC-10 were 52°, 53° and 59°, showing certain possible influence of the fibre dosage. As concerns to the model, the reproduction of this trajectories compared with those obtained in the experimental results can be seen in Figure 9. Considering the influence of the presence of particular fibres, the main direction of the cracks seemed to be reasonably captured by the simulation.

Let us now analyse the differences between the softening functions used in each case. Regarding the first point of the trilinear function, point $t$, it seems to be constant for different fibre dosages, since it remains

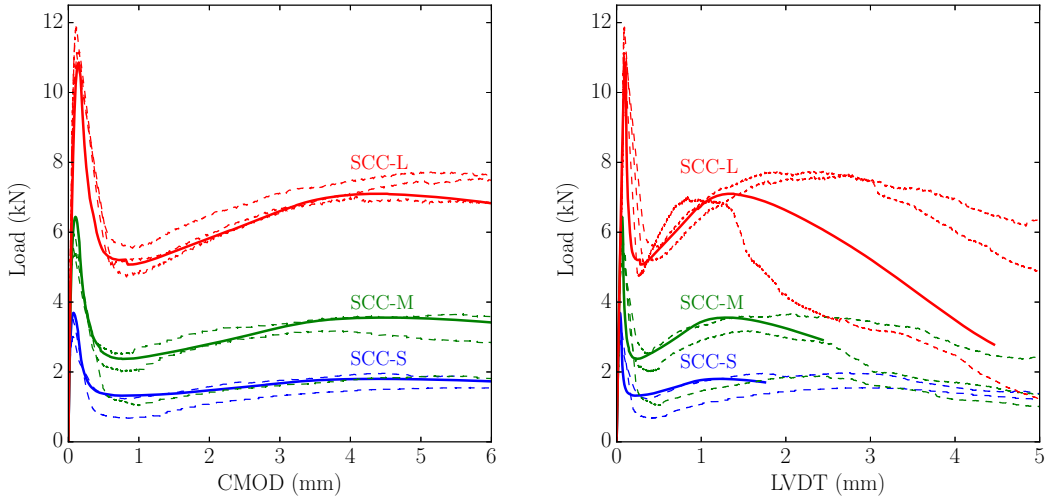


Figure 8: Load-CMOD and Load-LVDT diagrams for the self-compacting concrete specimens and simulations. Continuous lines represent the numerical results and dashed lines the experimental results.

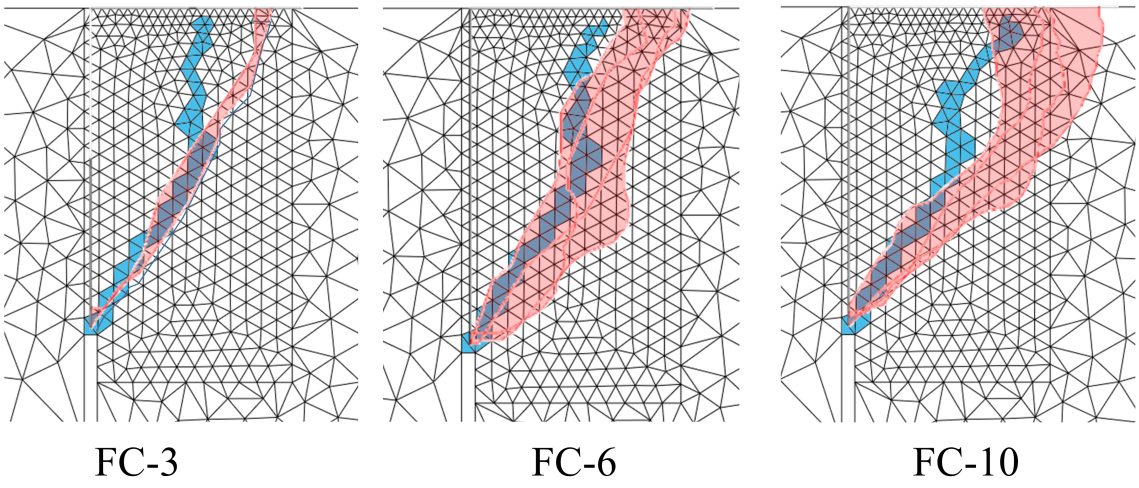


Figure 9: Comparison of the crack trajectories between the model (in blue) and the experimental results (in red).

constant for all the FC simulations, though must be adjusted if a different concrete proportioning is used. As regards the point $r$, which identifies the crack opening at which the action of fibres reduce its effectiveness, it is interesting to observe that it is positioned at a smaller value of $w$ with SCC simulations ($w = 1.65$ mm) and at a higher value with FC simulations ($w = 2.25$ mm). It must be noted that SCC specimens were manufactured with 48 mm long fibres and in their simulations point $r$ is positioned at $w = 1.65$ mm while FC specimens, manufactured with 60 mm long fibres, point $r$ is at $w = 2.25$ mm. This suggests that the influence of polyolefin fibres is extended when longer fibres are employed, which agrees well with what was observed in [24].

In order to understand the reinforcement mechanics of the fibres, a fracture surface analysis was performed. The results showed that 46%, 48% and 54% of the fibres were pulled out respectively for FC-3, FC-6 and FC-10. Previous research has shown that this value is around 40% in Mode I [32], showing a slight increment in the percentage of pulled-out fibres under mixed-mode and an increasing trend with the fibre dosage.

## 6. Conclusions

This study has checked the validity of trilinear softening functions on specimens tested under a three-point bending disposition that induces fracture under a combination of modes I and II. Six sets of experimental results have been used for comparison, envolving two types of concrete (FC and SCC), two lengths of polyolefin fibres (48 and 60 mm) and three proportions of fibres (3, 6 and 10 kg/m$^3$).

The main conclusions can be summarised as follows:

- A central forces cohesive approach has provided accurate numerical comparison with specimens tested under a loading setup that induces fracture combining modes I and II.
- The use of the cohesive zone approach by means of an embedded crack formulation with a trilinear softening function provides successful results under mixed-mode fracture conditions.
- Different concrete proportionings may require distinct $f_{ct}$ values when defining the characteristic points of the trilinear function.
- Using longer polyolefin fibres extends the action of fibres in the mix, leading to increasing loads at wider crack openings. This effect may be assessed by inverse analysis with the constitutive model of the composite material.
- The same softening function may be employed for different specimen sizes manufactured with the same fibre dosage, at least between the size ranges used in this study.

## Acknowledgements

The authors wish to express their gratitude to the finantial support provided for this research by the Ministry of Economy and Competitiveness of Spain by means of the Research Fund Project BIA2016-78742-C2-2-R.

## References

[1] Bentur A, Mindess S. Fibre reinforced cementitious composites. CRC Press; 2014.

[2] Banthia N, Gupta R. Influence of polypropylene fiber geometry on plastic shrinkage cracking in concrete. Cement and Concrete Research. 2006;36(7):1263 – 1267. Available from: http://www.sciencedirect.com/science/article/pii/S0008884606000056.

[3] Zollo RF. Fiber-reinforced concrete: an overview after 30 years of development. Cement and Concrete Composites. 1997;19(2):107 – 122. Available from: http://www.sciencedirect.com/science/article/pii/S0958946596000467.

[4] Khalid FS, Irwan JM, Ibrahim MHW, Othman N, Shahidan S. Performance of plastic wastes in fiber-reinforced concrete beams. Construction and Building Materials. 2018;183:451 – 464. Available from: http://www.sciencedirect.com/science/article/pii/S0950061818315204.

[5] Li B, Chi Y, Xu L, Shi Y, Li C. Experimental investigation on the flexural behavior of steel-polypropylene hybrid fiber reinforced concrete. Construction and Building Materials. 2018;191:80 – 94. Available from: http://www.sciencedirect.com/science/article/pii/S0950061818323894.

[6] Wang J, Dai Q, Si R, Guo S. Investigation of properties and performances of Polyvinyl Alcohol (PVA) fiber-reinforced rubber concrete. Construction and Building Materials. 2018;193:631 – 642. Available from: http://www.sciencedirect.com/science/article/pii/S0950061818326655.

[7] Brandt AM. Fibre reinforced cement-based (FRC) composites after over 40 years of development in building and civil engineering. Composite Structures. 2008;86(1):3 – 9. Fourteenth International Conference on Composite Structures. Available from: http://www.sciencedirect.com/science/article/pii/S0263822308000597.

[8] Beverly P. fib model code for concrete structures 2010. Ernst & Sohn; 2013.

[9] Instrucción de Hormigón Estructural EHE-08. Ministerio de Fomento, Madrid, España. 2008;.

[10] Alberti MG, Enfedaque A, Gálvez JC, Cánovas MF, Osorio IR. Polyolefin fiber-reinforced concrete enhanced with steel-hooked fibers in low proportions. Materials & Design. 2014;60:57 – 65. Available from: http://www.sciencedirect.com/science/article/pii/S026130691400243X.

[11] Enfedaque A, Alberti MG, Paredes JA, Gálvez JC. Interface properties of polyolefin fibres embedded in self-compacting concrete with a bond improver admixture. Theoretical and Applied Fracture Mechanics. 2017;90:287 – 293. Available from: http://www.sciencedirect.com/science/article/pii/S0167844217302446.

[12] Alberti MG, Enfedaque A, Gálvez JC. On the mechanical properties and fracture behavior of polyolefin fiber-reinforced self-compacting concrete. Construction and Building Materials. 2014;55:274 – 288. Available from: http://www.sciencedirect.com/science/article/pii/S0950061814000488.

[13] Alberti MG, Enfedaque A, Gálvez JC. Fracture mechanics of polyolefin fibre reinforced concrete: Study of the influence of the concrete properties, casting procedures, the fibre length and specimen size. Engineering Fracture Mechanics. 2016;154:225 – 244. Available from: http://www.sciencedirect.com/science/article/pii/S0013794415007201.

[14] Alberti MG, Enfedaque A, Gálvez JC. Fibre reinforced concrete with a combination of polyolefin and steel-hooked fibres. Composite Structures. 2017;171:317 – 325. Available from: http://www.sciencedirect.com/science/article/pii/S0263822316323741.

[15] Alberti MG, Enfedaque A, Gálvez JC. On the prediction of the orientation factor and fibre distribution of steel and macro-synthetic fibres for fibre-reinforced concrete. Cement and Concrete Composites. 2017;77:29 – 48. Available from: http://www.sciencedirect.com/science/article/pii/S0958946516307569.

[16] RILEM. Determination of the Fracture Energy of Mortar and Concrete by Means of Three-Point Bend Tests on Notched Beams. *Mater Struct*. 1985;18(106):285–290.

[17] Alberti MG, Enfedaque A, Gálvez JC, Reyes E. Numerical modelling of the fracture of polyolefin fibre reinforced concrete by using a cohesive fracture approach. Composites Part B: Engineering. 2017;111:200 – 210. Available from: http://www.sciencedirect.com/science/article/pii/S1359836816313567.

[18] Enfedaque A, Alberti MG, Gálvez JC, Domingo J. Numerical simulation of the fracture behaviour of glass fibre reinforced cement. Construction and Building Materials. 2017;136:108 – 117. Available from: http://www.sciencedirect.com/science/article/pii/S0950061816320517.

[19] Carpinteri A, Brighenti R. Fracture behaviour of plain and fiber-reinforced concrete with different water content under mixed mode loading. Materials & Design. 2010;31(4):2032–2042.

[20] Razmi A, Mirsayar M. On the mixed mode I/II fracture properties of jute fiber-reinforced concrete. Construction and Building Materials. 2017;148:512–520.

[21] Gálvez JC, Elices M, Guinea G, Planas J. Mixed mode fracture of concrete under proportional and nonproportional loading. *Int J Fract*. 1998;94(3):267–284.

[22] Gálvez JC, Planas J, Sancho JM, Reyes E, Cendón DA, Casati MJ. An embedded cohesive crack model for finite element analysis of quasi-brittle materials. *Eng Fract Mech*. 2013;109:369–386.

[23] Alberti MG, Enfedaque A, Gálvez JC, Agrawal V. Fibre distribution and orientation of macro-synthetic polyolefin fibre reinforced concrete elements. Construction and Building Materials. 2016;122:505 – 517. Available from: http://www.sciencedirect.com/science/article/pii/S0950061816310121.

[24] Alberti MG, Enfedaque A, Gálvez JC, Ferreras A. Pull-out behaviour and interface critical parameters of polyolefin fibres embedded in mortar and self-compacting concrete matrixes. Construction and Building Materials. 2016;112:607 – 622. Available from: http://www.sciencedirect.com/science/article/pii/S0950061816301878.

[25] Alberti MG, Enfedaque A, Gálvez JC. A review on the assessment and prediction of the orientation and distribution of fibres for concrete. Composites Part B: Engineering. 2018;151:274 – 290. Available from: http://www.sciencedirect.com/science/article/pii/S1359836817344001.

[26] Sancho JM, Planas J, Cendón DA, Reyes E, Gálvez JC. An embedded crack model for finite element analysis of concrete fracture. Engineering Fracture Mechanics. 2007;74(1):75 – 86. Fracture of Concrete Materials and Structures. Available from: http://www.sciencedirect.com/science/article/pii/S0013794406000488.

[27] Reyes E, Gálvez JC, Casati MJ, Cendón DA, Sancho JM, Planas J. An embedded cohesive crack model for finite element analysis of brickwork masonry fracture. Engineering Fracture Mechanics. 2009;76(12):1930 – 1944. Available from: http://www.sciencedirect.com/science/article/pii/S0013794409001490.

[28] Dugdale DS. Yielding of steel sheets containing slits. *J Mech Phys Solids*. 1960;8(2):100–104.

[29] Barenblatt GI. The Mathematical Theory of Equilibrium Cracks in Brittle Fracture. vol. 7 of *Adv Appl Mech*. Elsevier; 1962. p. 55–129.

[30] Hillerborg A, Modéer M, Petersson PE. Analysis of crack formation and crack growth in concrete by means of fracture mechanics and finite elements. *Cem Concr Res*. 1976;6(6):773 – 781.

[31] Bazant ZP, Planas J. *Fracture and size effect in concrete and other quasibrittle materials*. CRC press; 1997.

[32] Alberti MG, Enfedaque A, Gálvez JC, Agrawal V. Reliability of polyolefin fibre reinforced concrete beyond laboratory sizes and construction procedures. Composite Structures. 2016;140:506 – 524. Available from: http://www.sciencedirect.com/science/article/pii/S0263822315011587.

Highlights

- A cohesive fracture model is adapted for modelling the mixed mode fracture of Polyolefin Fibre Reinforced Concrete (PFRC).
- A trilinear softening function is fitted by means of inverse analysis for modelling the mixed mode fracture of PFRC.
- The trilinear softening function is included in embedded crack cohesive finite element.
- The proposed numerical model accurately predicts the mixed mode fracture of PFRC with distinct dosages of fibres.
- In addition, the cohesive embedded crack model properly fit the size effect shown by three homothetic PFRC specimens.